AgriEngineering

MDPI

Article

Differentiating Growth Patterns in Winter Wheat Cultivars via Unmanned Aerial Vehicle Imaging

Asparuh I. Atanasov [1], Hristo P. Stoyanov [2] and Atanas Z. Atanasov [3,*]

[1] Department of Mechanics and Elements of Machines, Technical University of Varna, 9010 Varna, Bulgaria; asparuh.atanasov@tu-varna.bg
[2] Dobrudzha Agricultural Institute General Toshevo, 9521 Petleshkovo, Bulgaria; hpstoyanov@abv.bg
[3] Department of Agricultural Machinery, Agrarian and Industrial Faculty, University of Ruse "Angel Kanchev", 7017 Ruse, Bulgaria
* Correspondence: aatanasov@uni-ruse.bg

Abstract: Wheat is one of the most widely grown cereal crops, serving as a key factor in sustaining the nutritional and food balance in numerous countries. The use of non-contact methods for wheat monitoring allows for the rapid diagnosis of vegetation density, crop growth, and the presence of weeds and diseases in the investigated fields. This study aims to assess the potential for differentiating growth patterns in winter wheat cultivars by examining them with two unmanned aerial vehicles (UAVs), the Mavic 2 Pro and Phantom 4 Pro, equipped with a multispectral camera from the MAPIR™ brand. Based on an experimental study conducted in the Southern Dobruja region (Bulgaria), vegetation reflectance indices, such as the Normalized-Difference Vegetation Index (NDVI), Soil-Adjusted Vegetation Index (SAVI), and Enhanced Vegetation Index 2 (EVI2), were generated, and a database was created to track their changing trends. The obtained results showed that the values of the NDVI, EVI2, and SAVI can be used to predict the productive potential of wheat, but only after accounting for the meteorological conditions of the respective growing season. The proposed methodology provides accurate results in small areas, with a resolution of 0.40 cm/pixel when flying at an altitude of 12 m and 2.3 cm/pixel when flying at an altitude of 100 m. The achieved precision in small and ultra-small agricultural areas, at a width of 1.2 m, will help wheat breeders conduct precise diagnostics of individual wheat varieties.

Keywords: agricultural monitoring; drones; infrared imaging; precision agriculture; vegetation indices

Citation: Atanasov, A.I.; Stoyanov, H.P.; Atanasov, A.Z. Differentiating Growth Patterns in Winter Wheat Cultivars via Unmanned Aerial Vehicle Imaging. *AgriEngineering* **2024**, *6*, 3652–3671. https://doi.org/10.3390/agriengineering6040208

Academic Editor: Mariano Crimaldi

Received: 17 August 2024
Revised: 27 September 2024
Accepted: 3 October 2024
Published: 7 October 2024

1. Introduction

Wheat is one of the most widespread cereal crops and upon which the nutrition of a large part of the world's population depends. Early forecasting of wheat yields is critical in calculating each country's food balance. One of the fastest and most economical ways to predict wheat yield is through the use of multispectral imagery obtained from unmanned aerial vehicles (UAVs). The aerial and satellite images obtained using remote-sensing techniques [1–3] are instrumental in analyzing the variability in agricultural crop reflectance. Spectral vegetation indices are extensively employed to monitor, analyze, and map changes in plant development, assess plant health, track phenological changes, estimate green biomass, and predict crop yield [4–6].

Some methods for extracting essential features from UAV images during critical growth stages important for winter wheat grain yield prediction have been proposed by Li, J et al. [7]. Crop phenotype monitoring using hyperspectral UAV imagery to classify different winter wheat cultivars is presented by Lyu, X et al. [8]. To optimize UAV flight strategies in the remote sensing of wheat, SPAD (Soil and Plant Analyzer Development) values were studied for the influence of UAV flight height on the accuracy of SPAD estimation [9]. An interesting approach is proposed by Zu, J et al. [10], which investigates the potential

of classical machine-learning models and deep-learning models to estimate the leaf area index (LAI) of winter wheat using multispectral images obtained from drones. Similar research on UAV-based hyperspectral and ensemble machine learning for predicting yield in winter wheat was conducted by Li, Z et al. [11]. A similar model for machine learning in faba bean breeding was proposed by [12]. An important condition for obtaining high wheat yields is favorable meteorological factors during the growing season. A model for diagnosing water stress of winter wheat by combining UAV multispectral and thermal remote sensing is presented by [13]. Other researchers [14] aim to predict seasonal genetic variation in cellular membrane thermostability (CMT), yield, and yield-related traits based on spectral data collected from UAVs. In addition to meteorological factors, the yield of wheat also depends on the fertility of the soil and its fertilization. Determining the amount of energy reflected from the surface of soil or plants in a certain spectral range is a widely used approach in agriculture. The factors that affect the degree of reflectance from the soil are reported by Baumgardner et al. [15]. A novel histogram separation threshold (HISET) methodology deriving spectral index soil-related thresholds and testing them for a Sentinel-2 temporal data stack is presented by [16]. In [17], the different detection methods, types, parts, and applications of remote-sensing (RS) techniques in soil measurements, as well as the advantages and disadvantages of the measurements of soil properties, are considered.

The use of UAVs for determining high-resolution Normalized-Difference Vegetation Index (NDVI) values in the application of fertilizers and the impact on the yields of rice and wheat crops was performed by Guan, S et al. [18]. A similar study on quantitative estimation of wheat phenotyping traits using ground and aerial imagery was presented by [19,20]. In addition to utilizing UAVs, some researchers [21] have predicted winter wheat yields by employing ground measurements, specifically using NDVI values obtained from GreenSeeker and MicaSense cameras. A thermographic method for assessing the adaptability of durum and common wheat varieties to the internal Mediterranean region of Italy was proposed by [22]. The possibility of monitoring the moisture in the upper soil layer using an unmanned aerial vehicle (UAV) was investigated, and the dynamics of the change in the Normalized Difference Water Index (NDWI) was determined by [23].

Analysis of previous studies reveals there is a very limited number of papers proposing a study on differentiating winter wheat growth patterns via UAV imaging. This gap is particularly evident in the context of specific geographic regions such as Southern Dobruja in Bulgaria. Our research aims to address this deficiency by providing a comprehensive methodology tailored to the unique conditions of Southern Dobruja, thus contributing valuable insights into the adaptability and growth patterns of winter wheat in this region.

The large-scale application of UAVs in agriculture is promising and is becoming one of the main ways to collect data on plant cultivation. Since the factors on which the growth of crops depends are strictly specific to a given region and are a variable value in individual years, analyzing the variations in individual wheat varieties requires long-term measurement throughout the growing season for each region.

The aim of this research is to explore the potential for differentiating winter wheat varieties using remote-sensing techniques with a small UAV and to investigate the correlation between spectral reflectance data and various phenological, biometric, and physiological indicators under specific agroclimatic conditions.

2. Materials and Methods

2.1. Plant Material

The experiment was conducted at the experimental field of the Dobrudjan Technological College in the city of Dobrich, Bulgaria, with coordinates 43.657963, 28.023110. The wheat (*Triticum aestivum* L.) varieties used in the experiment were Avenue, Annapurna (selection of Limagrain, Saint-Beauzire, France), Enola, and Merilin (selection of the Dobrudjan Agricultural Institute, Petleshkovo, Bulgaria). In the previous 2 growing seasons, the field was sown with winter cereals [24,25]. Pre-sowing field preparation was performed with a rotary tiller before sowing. Sowing was performed manually with an inter-row

distance of 30 cm and an intra-row distance of 15 cm on 4 November 2021 and 16 November 2022. No subsequent treatments were carried out during the growing season. The field was not treated with plant protection products.

2.2. Photographing the Experimental Plot and Calculating Vegetation Indices

During the observation period, 24,900 photographs were taken of the observed field. During the 2021–2022 season, from November to July, 19 recordings were conducted at intervals of 7 to 10 days. Similarly, during the 2022–2023 season, from November to July, 20 recordings were made at intervals of 7 to 10 days [26,27].

Data on vegetation index change trends were collected using a Red + Green + NIR (RGN, NDVI) MAPIR Survey3W Camera [28] with a 12-megapixel (4000 × 3000 px) Sony Exmor R IMX117 sensor. This Red + Green + NIR (RGN, NDVI) camera detects near-infrared radiation at a wavelength of 850 nm with a weighting coefficient of 0.0722, as well as red reflectance at 660 nm (0.2126) and green reflectance at 550 nm (0.7152). It features a Bayer RGB filter sensor and uses two green pixels for every red and blue pixel. In this setup, the blue pixel is replaced to detect near-infrared light.

During the experiment conducted in 2021–2022, the camera was mounted on a DJI Mavic 2 Pro UAV model manufactured by DJI (Da-Jiang Innovations, Shenzhen, China), as illustrated in Figure 1a [29]. In the 2022–2023 research period, the drone used for the observations was replaced with a DJI Phantom 4 Pro manufactured by DJI (Da-Jiang Innovations, Shenzhen, China), as shown in Figure 1b [29], serving as the camera platform. The software used to plan and perform the flights was Pix4Dcapture [30]. Due to the small size of the experimental areas, the flight height was set at 12 m above the terrain and a predetermined overlap of 80% in both the x and y directions. An example picture of the field in RGB and RGN spectra, divided into four blocks and the paths between them, as well as a generated NDVI index are shown in Figure 2 for 5 May 2023. On the RGB image in the visible range, no major development deviations are visible. The RGN photo provides similar information. On the generated NDVI map, the red areas with much lower vegetation are very clearly visible. It can be concluded that on the date of filming, the best vegetation is variety 3—Enola.

(**a**) (**b**)

Figure 1. UAV DJI Mavic 2 Pro, MAPIR Survey3W Camera (**a**). DJI Phantom 4 Pro, MAPIR Survey3W Camera (**b**).

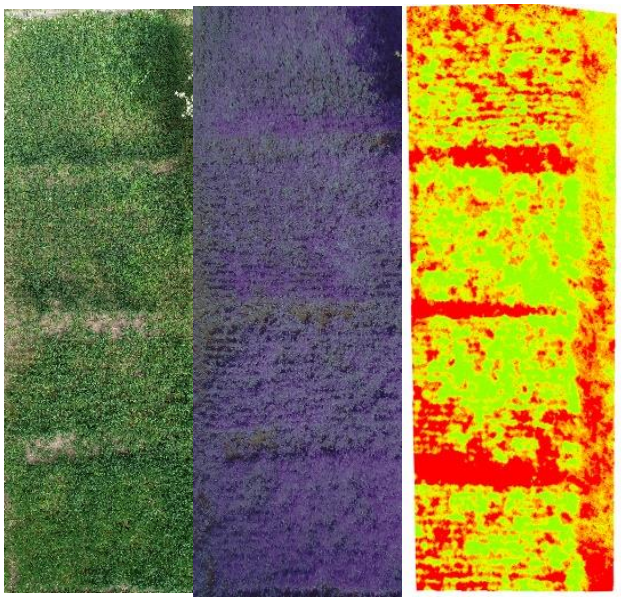

(**a**) (**b**) (**c**)

Figure 2. RGB image of the field (**a**), RGN image of the field (**b**), and generated NDVI (**c**).

Methods for vegetative indices included the following:

1. The obtained multispectral images were processed using the Pix4Dmapper software, version 4.4.12 [30]. Due to the set flight height and the resolution of the camera used, an average ground sampling distance (GSD) of 0.40 cm pixel^{-1} was obtained.

2. The indices were calculated based on the numerical values of the red and infrared reflectance. To obtain the numerical values of the colors in the individual fields, the photographs were cropped to a size that contained only one of the observed cultivars using the ImageJ software, Version 1.54 [31]. If the areas adjacent to the cultivar were not cropped from the image, summary data for the entire frame, including all cultivars present within it, will be obtained. Numerical values were generated from this image. The value of each color varies from 0 to 255. In Figure 3, in addition to the numerical values of the colors, the histogram of colors by reflectance spectra can be observed: green for G, red for R, and blue for NIR. Due to the specifics of the software, a blue channel is displayed instead of infrared, but comparison with the graph shows that the histogram corresponds to the spectral characteristics of the camera [28], in which the blue channel is repositioned in the near-infrared region and is 40 nm wide, unlike the other two, which are 20 nm wide. Using the numerical values of the colors, the vegetation index for this zone is calculated, the mathematical interpretations of which are reflected in the formulas indicated in Table 1.

Table 1. Spectral vegetation indices used to evaluate varieties of common winter wheat.

Index	Formula	Reference
NDVI	$(nir - red)/(nir + red)$	[32]
SAVI	$(nir - red)/((nir + red) \times (1 + 1/2))$	[33]
EVI2	$2.5 \times ((nir - red)/(nir + 2.4 \times red + 1))$	[34]

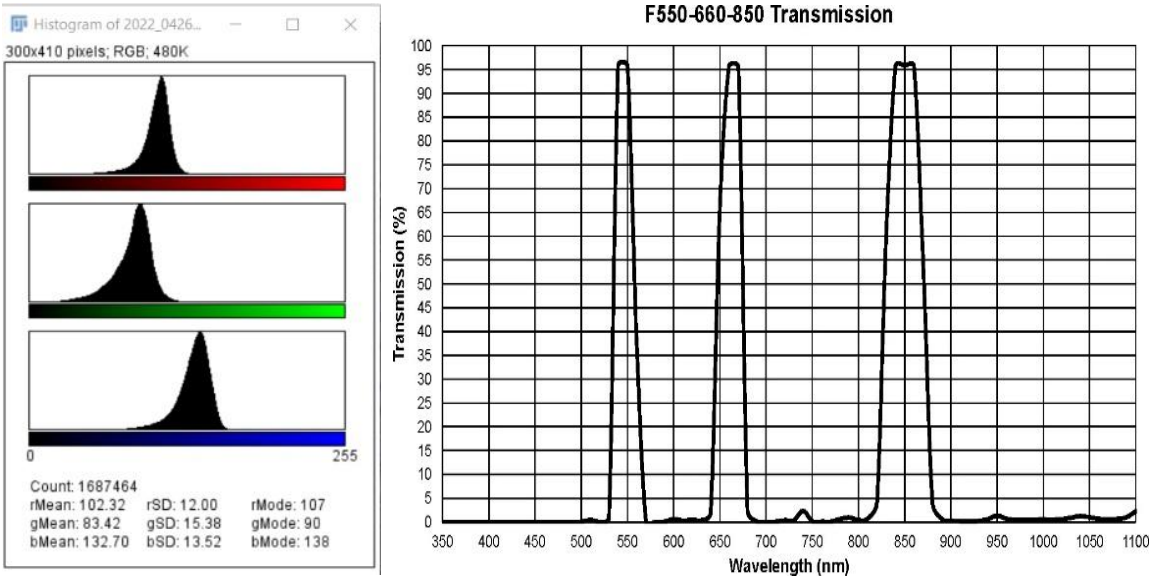

Figure 3. Spectral characteristics and numerical value of colors extracted from one plot (**a**) and spectral characteristics of the MAPIR camera (**b**).

2.3. Biometric Data and Statistical Analyses

From each of the varieties, the fully ripe spikelets were selected. Spike length, number of spikelets per spike, number of kernels per spike, kernel mass per spike, and the thousand-kernel weight were determined. The data are summarized and averaged by genotype and vegetation indices. Trends in the changes in the values of the specified parameters and the dependencies between them were evaluated. The relationships between each of the biometric indicators and the values of the spectral vegetation indices for each recording were established through a correlation analysis conducted in both vegetation years. Statistical data processing was performed using the software IBM SPSS Statistics—26 [35].

3. Results and Discussion

3.1. Weather Results

Regarding the phenological development, regardless of genotype, in both harvest years, the wheat varieties developed optimally, exhibiting no significant deviations from the characteristic features of the standard crops. Figure 4 shows the development of wheat over time in the 2021–2022 season.

Figure 4. The development of winter wheat during the vegetation stage for the 2021–2022 season.

During the data collection in the experimental field, the following meteorological parameters were recorded: wind speed (m/s), wind direction, air humidity (%), illumination (lx), temperature (°C), solar peak radiation (nm), cloud cover (%), color temperature (K), and illuminance (W m^{-2}). All meteorological data were analyzed to derive the existing relationships.

The presented data for the average monthly temperature and total monthly precipitation (Figures 5 and 6) highlight the highly contrasting nature of the two studied periods. Significant differences compared to the weather conditions characteristic of the region in terms of temperature were observed during the December–March period, and in precipitation in the months of December–January and May–June. The differences in these periods are sufficient to conclude that the vegetation in individual years proceeded in a distinct manner. During the individual research periods, such phenomena and processes can be clearly distinguished in terms of temperature and precipitation, which have a single manifestation but significantly affect the development of plants in the corresponding harvest year.

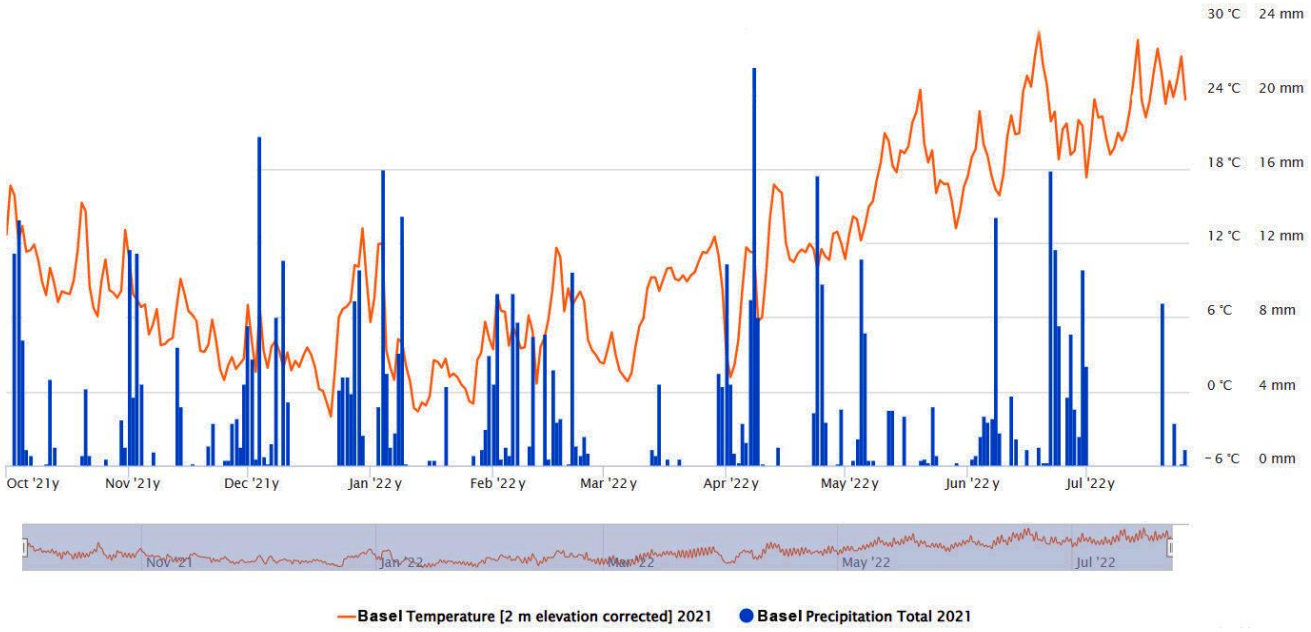

Figure 5. Air temperature and precipitation for the 2021–2022 growing season [36].

The weather conditions of the 2022–2023 growing season stand out the most, characterized by practically no rainfall for almost the whole of June, which hindered the proper filling of the grain, especially for the early varieties, which should complete their vegetation earlier. Another significant feature is the severe cold in the month of March 2021–2022, coupled with insufficient snow cover, which resulted in significant stress for the plants. The conditions of 2022 stand out as the most favorable for the growth and development of triticale, as the lowest number of negative weather events to cause stress are observed.

In terms of filming, the main limiting factor in Southern Dobruja is the wind. According to the Phantom 4 Pro's specifications, it has a maximum wind resistance of 10 m s^{-1}. On the Mavic 2 Pro, it is 8–10 m s^{-1}. Due to the installed additional camera, the mass of the UAV increases, which reduces the flight time but enhances resistance to wind gusts. The planning and implementation of the filming were in accordance with the weather forecast, avoiding days with wind over 10 m s^{-1}. At gusts above 8 m s^{-1}, a slight deviation from the flight path was observed, which the drone software compensated for instantly. In practice, during the periods of recording and carrying out the experimental activity, no days with wind speed above 10 m s^{-1} were observed, providing additional assurance of the quality of the received images.

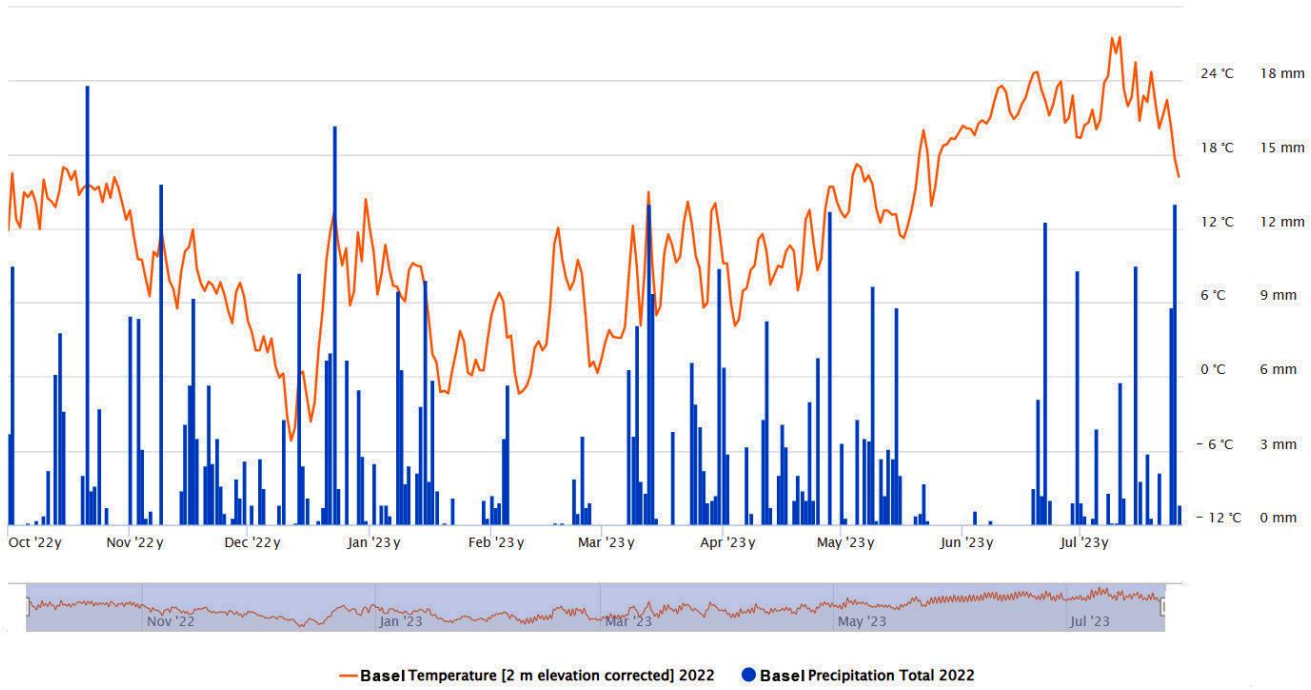

Figure 6. Air temperature and precipitation for the 2022–2023 growing season [36].

The aerial surveys were conducted at midday between 12:00 and 14:00 h when the sun was at its zenith. At this time, the effect of shadows was minimized as much as possible.

In the study using the DJI Mavic 2 Pro, 0.059% of the flights conducted over the observed field were unsuccessful due to wind gusts. For the test flights with the DJI Phantom 4 Pro, there were no unsuccessful flights. There was one flight affected by the wind, but despite the change in the flight path, data for the observed field were nevertheless collected.

3.2. Spectral Indices and Trends in the Studied Genotypes

The obtained results for the trends of change in the NDVI index of the four varieties in the 2021–2022 season demonstrate the relatively similar development of the four genotypes in terms of their vegetation development. Comparatively lower values compared to the other three varieties show Merilin had a slower rate of development in the initial phases, which is attributed to its characteristic feature of being greener and less waxy compared to the others (except for Enola). In the later phases, the spikes begin to exhibit a characteristic color with predominant red hues. While, in the early periods, rather low values of NIR are observed, compared to the other spectral characteristics, during the later stages for this variety, the high values of the red part of the spectrum prevail. A specific feature during the same vegetation period is the sharp change in NDVI values, which gives a sudden change in the curve of the dynamics of this parameter. This is associated with the lack of moisture storage in certain periods and the intensity and amount of precipitation (Figure 7). In the absence of sufficient moisture, growth and development slow down significantly, which leads to the death of the leaves and an increase in the red spectrum. Accordingly, similar effects are associated with a sharp decrease in NDVI values. On the other hand, both intensive growth in the early periods and accelerated vegetation imply a decrease in the levels of the red part of the spectrum, which in turn leads to an increase in NDVI values. For this reason, the presence of sufficient moisture in the soil and intense rainfall lead to an increase in the values of the indicator for all investigated varieties, and in the absence of rainfall (mid-May 2022–early June 2022), the NDVI values decrease. As plants died just before harvest, NDVI values decreased for all cultivars. The highest value was for the Avenue variety, which in the same season reacts relatively less to rainfall, as it is

earlier and enters the maturity phase earlier. On the other hand, the intense wax coating of the variety and the absence of wasps are associated with higher index values in the same period. For comparison and verification of the accuracy of the results, the EVI2 and SAVI are shown in Figure 8. There is a complete coincidence of the changing trends of the curve of each variety, although the numerical values for the different indices are not the same.

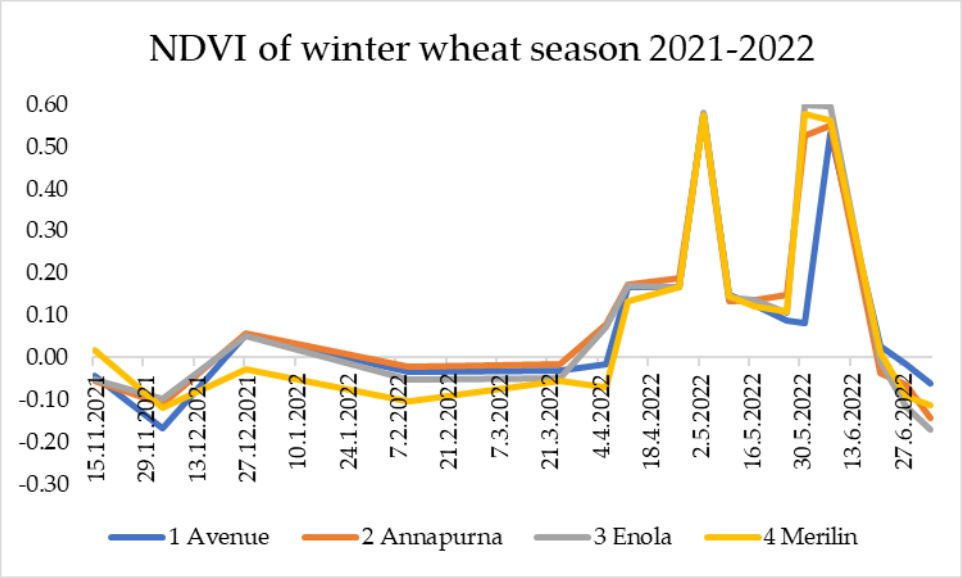

Figure 7. Trends of NDVI change by variety for the 2021/2022 growing season.

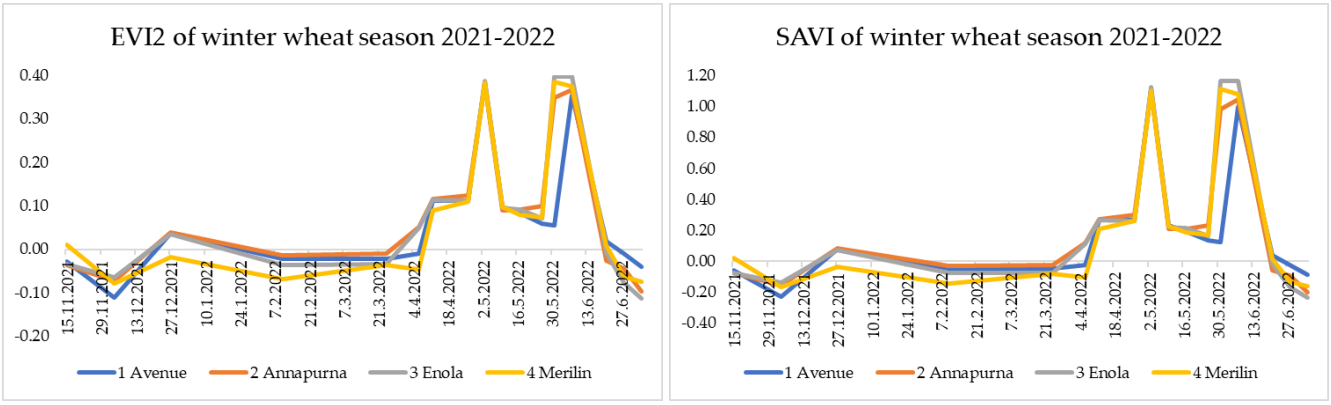

(**a**) (**b**)

Figure 8. Trends of changes in the EVI2 (**a**) and SAVI (**b**) by variety for 2021–2022 throughout the growing season.

The obtained trends are also confirmed for the 2022–2023 growing season (Figure 9). The Avenue variety is distinguished by its significantly earlier development, as evidenced by the faster increase in NDVI values in the February–March period. Notably, the varieties are significantly differentiated from the middle of December 2022 to the end of the first ten days of April 2023. After this period, differences in the dynamics of change in NDVI values are almost absent, and if present, they are negligibly small. During the December–January period, the highest NDVI values are observed in Merilin, followed by Avenue, and the lowest in Enola and Annapurna, respectively. This indicates that Avenue and Merilin develop relatively intensively during the winter period, no frost damage is observed, and they form a relatively dense crop. On the other hand, Enola and Annapurna develop less during the winter period and accumulate less biomass, which leads to lower NDVI values. However, in the month of February, both varieties managed to develop, albeit at a slower

pace. In the following periods, the change in the three varieties is identical, while Avenue differs significantly due to its faster development. The changes in the EVI2 and SAVI for the same period are also similar (Figure 10). The only notable difference is observed just before maturity, where the values of the EVI2 and SAVI in the Merilin cultivar are significantly lower. This is again attributed to the red coloration of the awns of the variety during this period.

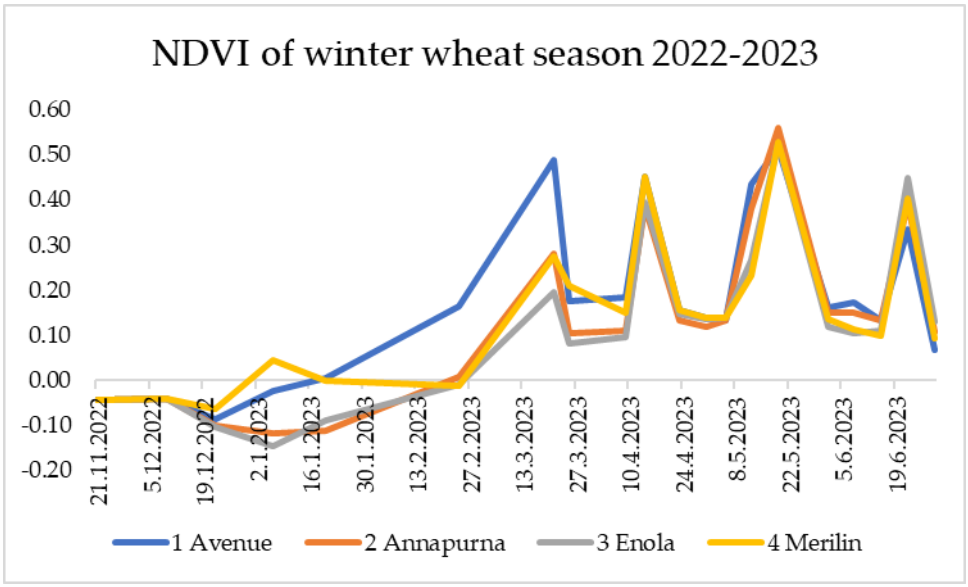

Figure 9. Trends of NDVI change by variety 2021–2022.

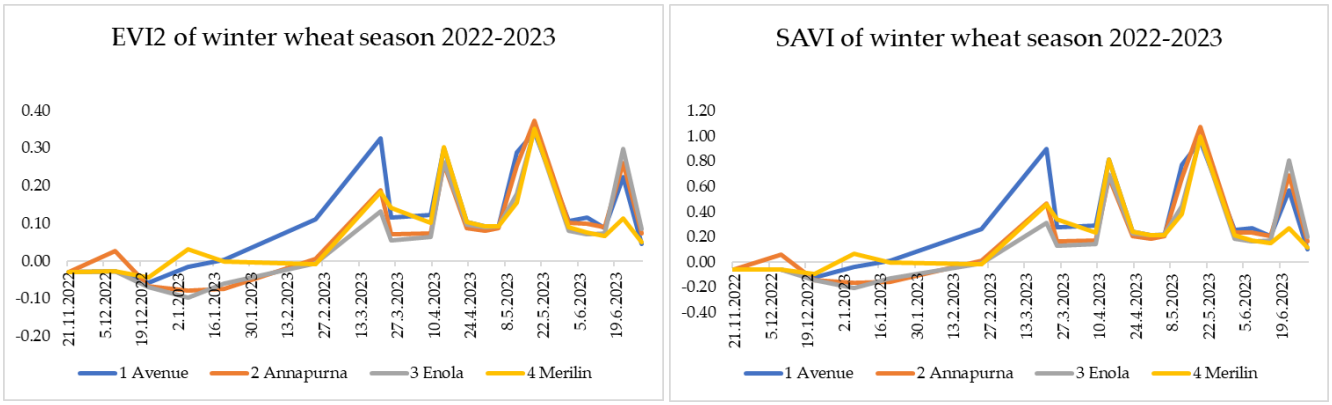

(**a**) (**b**)

Figure 10. Trends of changes in the EVI2 (**a**) and SAVI (**b**) by variety for 2022–2023 throughout the growing season.

3.3. Biometric Indicators and Trends in the Studied Genotypes

The data on the biometric indicators for the studied varieties, summarized in Table 2, reveal that the values vary depending on the study period. This variation is attributed to differences in meteorological conditions across the two growing seasons, as well as the response of the respective genotypes to the specific conditions of each growing season.

Table 2. Data on biometric indicators for the studied genotypes by year and average for the period.

G		**Merilin**			**Annapurna**	
E	2021/2022	2022/2023	Average	2021/2022	2022/2023	Average
LS	8.46 b	7.47 ab	8.07 b	8.29 b	7.05 a	7.93 b
NSS	18 a	15 a	17 a	17 a	15 a	17 a
NGS	44 b	29 a	38 b	42 b	37 bc	40 bc
WGS	1.69 b	1.04 a	1.44 b	1.69 b	1.26 b	1.57 c
M1000	38.32 b	36.52 c	37.62 bc	40.57 c	34.25 c	38.73 c
G		**Avenue**			**Enola**	
E	2021/2022	2022/2023	Average	2021/2022	2022/2023	Average
LS	7.36 a	7.73 b	7.51 a	9.12 c	10.04 c	9.52 c
NSS	17 a	17 b	17 a	18 a	20 c	19 b
NGS	36 a	33 b	35 a	43 b	39 c	41 c
WGS	1.19 a	1.01 a	1.12 a	1.90 c	1.05 a	1.53 bc
M1000	33.24 a	30.67 b	32.16 a	44.31 d	25.77 a	36.25 b

The reliable differences for each indicator are between the individual genotypes by year and on average for the studied period. LS represents the length of the spike, NSS is the number of spikelets per spike, NGS is the number of grains per spike, WGS is the weight of grains per spike, and M1000 is the thousand-kernel weight.

Regarding spike length, the Enola variety exhibited the highest values in the 2021–2022 growing season, while the Avenue variety had the lowest values, reliably distinguishing itself from the other two varieties. In the subsequent growing season, Enola continued to form the longest spikes, but the other three varieties were not reliably distinguished from one another. On average, over the study period, the values followed the trend established during the first growing season: Enola consistently had the longest spikes, followed by Merilin and Annapurna, with Avenue showing the shortest spikes.

The number of spikelets per spike is a significantly more stable indicator than spike length. During the 2021–2022 growing season, no significant differences were observed among the varieties. This indicates that spike length was not a decisive factor for the number of spikelets formed or, consequently, for the number of grains per spike in this research year. In the subsequent growing season, the Merilin and Annapurna varieties had the lowest number of spikelets per spike, followed by Avenue, while the Enola variety exhibited the highest number. Over the study period, the Avenue, Merilin, and Annapurna varieties did not show statistically significant differences in this indicator, whereas the Enola variety had a significantly higher number of spikelets per spike.

The number of grains per spike exhibits much greater variability compared to the previous two indicators. This is largely due to the strong dependence of the pollination and fertilization processes on air temperature and precipitation during the relevant growing season. In the 2021–2022 growing season, the highest values were recorded for the Merilin variety, which did not show statistically significant differences from the Annapurna and Enola varieties. Only the Avenue variety had a significantly lower grain yield. In the following growing season, the highest values for this indicator were observed in the Enola variety. Similar grain formation was observed in the Annapurna variety. Significantly lower results were reported for Avenue, with the lowest recorded for Merilin. On average, over the study period, the weakest pollination was observed in Avenue, followed by Merilin. The highest results were recorded in Enola, which did not show statistically significant differences from Annapurna.

A similar and dynamic trend is observed concerning the indicator for the mass of grains per spike. During the 2021–2022 season, the highest values were recorded for the Enola variety, while the lowest were observed for the Avenue variety, which was statistically distinct from the other two varieties. No significant differences were reported between Merilin and Annapurna. In the 2022–2023 growing season, no reliable differences were observed among Merilin, Avenue, and Enola, as the values were too similar. Only the Annapurna variety exhibited a distinct difference. On average, over the study period,

the highest yield, as indicated by the mass of grains per spike, was recorded for Enola, with similar values observed for Annapurna. Lower results were obtained for the Merilin variety and the lowest for the Avenue variety. These trends demonstrate that grain mass per spike is an extremely complex parameter, significantly influenced by environmental conditions. The low values can be attributed to both a lower number of grains per spike and a lower mass per 1000 grains. This indicates that unfavorable conditions during the flowering period (May) and the grain-filling period (May–June) have a substantial impact. Significant differences in moisture availability were observed during both periods. The low values of the indicator in the 2023 growing season are directly associated with the lack of precipitation in June of the same year.

Evidence for the above statement is provided by the values of the 1000-grain mass indicator across the two research years for all studied genotypes. In the 2021–2022 growing season, the values were significantly higher than those in 2022–2023. However, different trends were observed for individual cultivars. In 2021–2022, the Enola variety exhibited the highest values for this indicator, followed reliably by Annapurna. Lower results were recorded for Merilin, with the Avenue variety showing the smallest grain mass. In the subsequent growing season, a markedly different trend was observed: the Enola variety had the lowest values, followed by Avenue, while Merilin and Annapurna exhibited significantly higher values. This can be attributed to the fact that Enola and Avenue are early varieties, with grain filling occurring at an earlier stage in the calendar year. Given that severe droughts occurred in 2023 after the beginning of June, both varieties experienced insufficient grain nourishment. The lack of moisture and higher temperatures led to premature ripening and smaller grain size. On average, over the two research years, the values more closely align with the trend observed in 2021–2022, which is characteristic of the varieties.

The features mentioned for the individual indicators are confirmed by the interrelationships observed between them for the different research years. During the first growing season (2021–2022), high and significant positive correlations were reported between the mass of kernels per ear and ear length, as well as between the thousand-kernel weight and spike length (see Table 3). This can be explained by the fact that larger spikes facilitate higher photosynthetic activity, which results in larger and better-nourished grains. A reliable correlation was also observed between the mass of grains in a row and the thousand-kernel weight. This suggests that larger grain size is associated with higher grain yield per spike. The mass of kernels per ear showed a high but not significant correlation with the number of kernels per ear. This indicates that while the number of grains is important for class productivity, this indicator varies among different genotypes, as established by the primary biometric results.

Table 3. Correlation dependencies between the studied biometric indicators for the growing season 2021–2022.

	LS	**NSS**	**NGS**	**WGS**	**M1000**
LS	1	0.712	0.890	0.981 *	0.956 **
NSS	0.712	1	0.588	0.586	0.501
NGS	0.890	0.588	1	0.934	0.804
WGS	0.981 *	0.586	0.934	1	0.963 *
M1000	0.956 **	0.501	0.804	0.963 *	1

LS represents the length of the spike, NSS is the number of spikelets per spike, NGS is the number of grains per spike, WGS is the weight of grains per spike, and M1000 is the thousand-kernel weight. Strong dependencies are indicated with an asterisk (*). Significance levels (p-values) are classified as follows: * $p = 0.05$; ** $p = 0.01$.

Table 3 shows that there is a strong correlation between the LS parameter with WGS and M1000. From this, we can form conclusions about the relationship of the two parameters with the reflective vegetation indices. In the following research year, high, reliable, and positive correlations were observed between the indicators of spike length and the number of spikelets per spike (see Table 4). This indicates that a larger number of spikelets

corresponds to a larger spike. The correlation between the number of spikelets per spike and the mass of 1000 grains is high, reliable, but negative. The correlation coefficients between the number of kernels per spike and the mass of 1000 kernels, as well as between the number of kernels per spike and spike length, are high but negative and unreliable. These values suggest that the number of spikes is a key indicator related to yield, on which both the number of grains per spike and their size largely depend. Larger grains are associated with a smaller number of spikelets and, correspondingly, with a smaller number of grains per spike. However, the unreliable correlations indicate that these dependencies vary among individual varieties, and each yield-related indicator has specific significance for the formation of class productivity.

Table 4. Correlational dependencies between the studied biometric indicators for the 2022–2023 growing season.

	LS	NSS	NGS	WGS	M1000
LS	1	0.958 **	0.602	−0.453	−0.892
NSS	0.958 **	1	0.708	−0.416	−0.983 *
NGS	0.602	0.708	1	0.337	−0.771
WGS	−0.453	−0.416	0.337	1	0.339
M1000	−0.892	−0.983 *	−0.771	0.339	1

LS represents the length of the spike, NSS is the number of spikelets per spike, NGS is the number of grains per spike, WGS is the weight of grains per spike, and M1000 is the thousand-kernel weight. Strong dependencies are indicated with an asterisk (*). Significance levels (p-values) are classified as follows: * $p = 0.05$; ** $p = 0.01$.

In Table 4, for the research year 2022–2023, a strong correlation can be observed between the NSS parameter and both LS and M1000.

The obtained results, both in relation to the individual studied indicators and the dependencies between them, demonstrate that each growing season is characterized by specific features that directly depend on meteorological factors (temperature and precipitation) and the response of the individual varieties. Consequently, it is important to investigate dependencies with spectral indices while accounting for the peculiarities of each growing season.

3.4. Relationship between Spectral Indices and Biometrics

Given the significant role of vegetative development and photosynthetic activity in achieving high productivity, it is expected that there will be certain relationships between vegetation spectral indices and biometric indicators during various phases of plant development. The results obtained for the correlation coefficients between the productivity-related indicators and the values of the NDVI, EVI2, and SAVI show that, in both growing seasons, specific relationships are observed, which logically reflect the processes of biomass growth and development.

In the 2021–2022 growing season (see Table 5), the highest reliable and positive correlations were reported between the number of grains per spike and the NDVI reported for 4 December 2021, 26 May 2022, and 31 May 2022; between the weight of grains per spike and the NDVI reported for 17 May 2022 and 31 May 2022; and between the thousand-kernel weight and the NDVI reported on 17 May 2022. Again, the correlations reported between the length of the spike and the NDVI for 28 June 22 and 05 July 22 and between the thousand-kernel weight and the NDVI for 28 June 22 and 05 July 22 are high and reliable but negative. The same trends, but with different values of the correlation coefficients, are observed for the other two vegetation spectral indices (Tables 6 and 7). Correlations of number of grains per spike in May can be explained by the fact that the more developed the vegetative mass of a cultivar, the larger the spikes that will be formed, and larger spikes are generally associated with more grain per ear. In this regard, it is logical that the number of grains per class correlates highly with the spectral indices in this time period. The correlation of the thousand-kernel weight with spectral indices during the recording period was mostly positive, being significant in the month of May, which again coincided

with the vegetative development of biomass, suggesting that higher plant biomass could be associated with a greater possibility of feeding the grain.

Table 5. Correlation dependencies between the studied biometric indicators and the NDVI by recording date in the 2021–2022 growing season.

	LS	NSS	NGS	WGS	M1000
NDVI 04.11.21	-	-	-	-	-
NDVI 15.11.21	0.477	0.560	0.775	0.510	0.260
NDVI 04.12.21	0.888	0.643	**0.997** **	0.920	0.781
NDVI 27.12.21	−0.054	−0.633	−0.231	0.023	0.240
NDVI 10.02.22	0.103	−0.541	−0.064	0.188	0.390
NDVI 24.03.22	0.244	−0.460	0.435	0.424	0.415
NDVI 05.04.22	0.088	−0.615	0.028	0.212	0.366
NDVI 06.04.22	0.438	−0.129	0.141	0.458	0.671
NDVI 12.04.22	−0.621	−0.889	−0.717	−0.558	−0.366
NDVI 26.04.22	0.705	0.038	0.786	0.826	0.808
NDVI 03.05.22	0.800	0.180	0.851	0.899	0.875
NDVI 10.05.22	0.094	−0.453	−0.168	0.136	0.373
NDVI 17.05.22	0.918	0.393	0.905	**0.975** *	**0.952** *
NDVI 25.05.22	0.336	−0.389	0.224	0.439	0.591
NDVI 26.05.22	0.750	0.452	**0.969** *	0.828	0.656
NDVI 31.05.22	0.897	0.518	**0.993** **	**0.954** *	0.845
NDVI 07.06.22	0.831	0.816	0.924	0.815	0.648
NDVI 21.06.22	−0.803	−0.157	−0.792	−0.891	−0.907
NDVI 28.06.22	**−0.997** **	−0.761	−0.881	**−0.966** *	**−0.936**
NDVI 05.07.22	**−0.988** *	−0.620	−0.932	**−0.999** **	**−0.961** *

LS represents the length of the spike, NSS is the number of spikelets per spike, NGS is the number of grains per spike, WGS is the weight of grains per spike, and M1000 is the thousand-kernel weight. Strong dependencies are indicated with an asterisk (*). The correlation levels are as follows: for LS, R ranges from 0.988 to 0.997; for NGS, R ranges from 0.969 to 0.997; for WGS, R ranges from 0.966 to 0.999; for M1000, R ranges from 0.936 to 0.961. Significance levels (p-values) are classified as follows: * $p = 0.05$; ** $p = 0.01$.

Table 6. Correlation dependencies between the studied biometric indicators and the EVI2 by recording date in the 2021–2022 growing season.

	LS	NSS	NGS	WGS	M1000
EVI2 04.11.21	-	-	-	-	-
EVI2 15.11.21	0.477	0.560	0.775	0.510	0.260
EVI2 04.12.21	0.888	0.643	**0.997** **	0.920	0.781
EVI2 27.12.21	−0.054	−0.633	−0.231	0.023	0.240
EVI2 10.02.22	0.103	−0.541	−0.064	0.188	0.390
EVI2 24.03.22	0.244	−0.460	0.435	0.424	0.415
EVI2 05.04.22	0.088	−0.615	0.028	0.212	0.366
EVI2 06.04.22	0.438	−0.129	0.141	0.458	0.671
EVI2 12.04.22	−0.621	−0.889	−0.717	−0.558	−0.366
EVI2 26.04.22	0.705	0.038	0.786	0.826	0.808
EVI2 03.05.22	0.800	0.180	0.851	0.899	0.875
EVI2 10.05.22	0.094	−0.453	−0.168	0.136	0.373
EVI2 17.05.22	0.918	0.393	0.905	0.975 *	**0.952** *
EVI2 25.05.22	0.336	−0.389	0.224	0.439	0.591
EVI2 26.05.22	0.750	0.452	**0.969** *	0.828	0.656
EVI2 31.05.22	0.897	0.518	**0.993** **	**0.954** *	0.845
EVI2 07.06.22	0.831	0.816	0.924	0.815	0.648
EVI2 21.06.22	−0.803	−0.157	−0.792	−0.891	−0.907

Table 6. *Cont.*

	LS	NSS	NGS	WGS	M1000
EVI2 28.06.22	**−0.997** **	−0.761	−0.881	**−0.966** *	−0.936
EVI2 05.07.22	−0.988 *	−0.620	−0.932	**−0.999** **	**−0.961** *

LS represents the length of the spike, NSS is the number of spikelets per spike, NGS is the number of grains per spike, WGS is the weight of grains per spike, and M1000 is the thousand-kernel weight. Strong dependencies are indicated with an asterisk (*). The correlation levels are as follows: for LS, R −0.997; for NGS, R ranges from 0.969 to 0.997; for WGS, R ranges from 0.966 to 0.999; for M1000, R ranges from 0.952 to 0.961. Significance levels (*p*-values) are classified as follows: * $p = 0.05$; ** $p = 0.01$.

Table 7. Correlational dependencies between the studied biometric indicators and the SAVI by recording date in the 2021–2022 growing season.

	LS	NSS	NGS	WGS	M1000
SAVI 04.11.21	-	-	-	-	-
SAVI 15.11.21	0.472	0.559	0.770	0.504	0.254
SAVI 04.12.21	0.887	0.647	**0.996** **	0.919	0.778
SAVI 27.12.21	−0.048	−0.630	−0.226	0.029	0.245
SAVI 10.02.22	0.106	−0.542	−0.058	0.192	0.391
SAVI 24.03.22	0.242	−0.463	0.433	0.422	0.413
SAVI 05.04.22	0.088	−0.616	0.032	0.213	0.365
SAVI 06.04.22	0.445	−0.123	0.149	0.465	0.676
SAVI 12.04.22	−0.624	−0.891	−0.718	−0.561	−0.370
SAVI 26.04.22	0.705	0.037	0.785	0.826	0.808
SAVI 03.05.22	0.800	0.180	0.850	0.899	0.876
SAVI 10.05.22	0.095	−0.453	−0.167	0.137	0.374
SAVI 17.05.22	0.917	0.392	0.904	**0.975** *	**0.953** *
SAVI 25.05.22	0.337	−0.388	0.225	0.440	0.592
SAVI 26.05.22	0.750	0.452	**0.969** *	0.828	0.656
SAVI 31.05.22	0.899	0.525	**0.994** **	**0.954** *	0.845
SAVI 07.06.22	0.826	0.816	0.922	0.810	0.642
SAVI 21.06.22	−0.805	−0.160	−0.794	−0.893	−0.907
SAVI 28.06.22	**−0.998** **	−0.757	−0.886	**−0.968** *	−0.936
SAVI 05.07.22	**−0.986** *	−0.616	−0.936	**−0.999** **	**−0.959** *

LS represents the length of the spike, NSS is the number of spikelets per spike, NGS is the number of grains per spike, WGS is the weight of grains per spike, and M1000 is the thousand-kernel weight. Strong dependencies are indicated with an asterisk (*). The correlation levels are as follows: for LS, R ranges from 0.986 to 0.998; for NGS, R ranges from 0.969 to 0.996; for WGS, R ranges from 0.954 to 0.999; for M1000, R ranges from 0.953 to 0.959. Significance levels (*p*-values) are classified as follows: * $p = 0.05$; ** $p = 0.01$.

After mid-June 2022, however, the dependencies become negative. This indicates that the earlier a cultivar matures and the faster its biomass dies, the less likely it is to produce larger grains. In this context, a longer preservation of green biomass is associated with larger grains. It should be noted that early ear formation and the onset of biological maturity are related, but not functionally; biomass dieback and early maturity may be related in different ways. The correlations between the mass of grains per row and the vegetation indices, including the number of grains per row and the thousand-kernel weight, follow a logical relationship. This suggests that productivity is directly related to vegetative development, as good vegetative development can help predict productivity. However, given that meteorological factors may cause sudden changes in biomass development, the values of vegetation indices should be interpreted with caution.

A typical example in this regard is the values of the correlation coefficients of the spectral vegetation indices in the agricultural year 2022–2023 (see Table 8). The majority of their values are low, unreliable, and negative, which shows that during this growing season, biometric indicators are related to the very large dynamics of meteorological elements, and the development of biomass can hardly be used as a guide for predicting productivity. During this research year, high, positive, and reliable correlations were recorded only between the weight of grains per spike and the NDVI for 23 April 2023 and 30 April

2023. High and significant correlations of the weight of grains per spike and the number of spikelets per spike with NDVI were negative. In this research year, it is noticeable that the correlation coefficients of the EVI2 and SAVI with the biometric characteristics of the studied varieties differ as a trend. In addition to the mentioned correlations, high correlation coefficients of the EVI2 and SAVI with the number of spikelets per spike for 22 June 2023 (Table 9) and with the weight of grains per spike for 9 December 2023 (Table 10) are observed. The first high correlation indicates that high photosynthetic activity is indirectly associated with better adaptability of the specific genotype. It was found that despite unfavorable environmental conditions, the ear of wheat formed more grain.

Table 8. Correlation dependencies between the studied biometric indicators and the NDVI by recording date in the 2022–2023 growing season.

	LS	NSS	NGS	WGS	M1000
NDVI 21.11.22	-	-	-	-	-
NDVI 09.12.22	-	-	-	-	-
NDVI 22.12.22	−0.401	−0.528	**−0.972** *	−0.530	0.617
NDVI 06.01.23	−0.528	−0.614	**−0.988** *	−0.462	0.672
NDVI 20.01.23	−0.275	−0.276	−0.813	−0.733	0.304
NDVI 24.02.23	−0.234	0.003	−0.141	−0.342	−0.127
NDVI 21.03.23	−0.458	−0.253	−0.371	−0.288	0.140
NDVI 25.03.23	−0.593	−0.664	**−0.989** *	−0.404	0.710
NDVI 09.04.23	−0.455	−0.363	−0.715	−0.538	0.326
NDVI 14.04.23	−0.286	−0.306	−0.844	−0.724	0.343
NDVI 23.04.23	0.194	0.143	−0.585	**−0.960** *	−0.066
NDVI 30.04.23	0.509	0.443	−0.318	**−0.993** **	−0.348
NDVI 05.05.23	0.588	0.339	−0.126	−0.477	−0.162
NDVI 12.05.23	−0.382	−0.103	0.221	0.268	−0.077
NDVI 19.05.23	−0.392	−0.398	0.326	0.987 *	0.348
NDVI 01.06.23	−0.821	−0.640	−0.417	0.187	0.510
NDVI 08.06.23	−0.509	−0.243	0.040	0.220	0.071
NDVI 15.06.23	−0.353	−0.083	0.379	0.463	−0.099
NDVI 22.06.23	0.711	0.526	0.467	0.037	−0.407
NDVI 29.06.23	0.626	0.523	0.731	0.351	−0.467

LS represents the length of the spike, NSS is the number of spikelets per spike, NGS is the number of grains per spike, WGS is the weight of grains per spike, and M1000 is the thousand-kernel weight. Strong dependencies are indicated with an asterisk (*). The correlation levels are as follows: for NGS, R ranges from 0.972 to 0.989; for WGS, R ranges from 0.960 to 0.993. Significance levels (p-values) are classified as follows: * $p = 0.05$; ** $p = 0.01$.

The second correlation indicates that early vegetative development of plants largely determines their subsequent growth. In this context, higher values of spectral indices at the beginning of the growing season are likely indicators of greater productivity, regardless of environmental conditions. However, the lack of significant correlations between spectral indices during this growing season underscores the thesis that considerable fluctuations in meteorological conditions can substantially influence trends in vegetative development.

The absence of any high and significant correlations between the thousand-kernel weight and any of the vegetation indices confirms the above thesis. In this regard, it can be considered that the values of the indices used in the study are important for predicting the productivity, but in strict compliance with the specific conditions of the growing season.

Table 9. Correlation dependencies between the studied biometric indicators and the EVI2 by recording date in the 2022–2023 growing season.

	LS	NSS	NGS	WGS	M1000
EVI2 21.11.22	-	-	-	-	-
EVI2 09.12.22	−0.509	−0.443	0.318	**0.993** **	0.348
EVI2 22.12.22	−0.377	−0.546	**−0.957** *	−0.460	0.655
EVI2 06.01.23	−0.530	−0.625	**−0.992** **	−0.446	0.688
EVI2 20.01.23	−0.305	−0.323	−0.851	−0.710	0.359
EVI2 24.02.23	−0.218	0.015	−0.150	−0.368	−0.136
EVI2 21.03.23	−0.463	−0.249	−0.336	−0.251	0.129
EVI2 25.03.23	−0.507	−0.568	**−0.968** *	−0.511	0.615
EVI2 09.04.23	−0.494	−0.410	−0.744	−0.509	0.375
EVI2 14.04.23	−0.406	−0.416	−0.881	−0.631	0.441
EVI2 23.04.23	0.509	0.443	−0.318	**−0.993** **	−0.348
EVI2 30.04.23	0.509	0.443	−0.318	**−0.993** **	−0.348
EVI2 05.05.23	-	-	-	-	-
EVI2 12.05.23	−0.399	−0.121	0.167	0.220	−0.056
EVI2 19.05.23	−0.337	−0.373	0.322	**0.965** *	0.341
EVI2 01.06.23	−0.707	−0.489	−0.281	0.145	0.342
EVI2 08.06.23	−0.686	−0.453	−0.159	0.253	0.293
EVI2 15.06.23	−0.588	−0.339	0.126	0.477	0.162
EVI2 22.06.23	0.555	0.701	**0.988** *	0.306	−0.785
EVI2 29.06.23	0.755	0.733	0.896	0.242	−0.714

LS represents the length of the spike, NSS is the number of spikelets per spike, NGS is the number of grains per spike, WGS is the weight of grains per spike, and M1000 is the thousand-kernel weight. Strong dependencies are indicated with an asterisk (*). The correlation levels are as follows: for NGS, R ranges from 0.957 to 0.988; for WGS, R ranges from 0.965 to 0.993. Significance levels (p-values) are classified as follows: * $p = 0.05$; ** $p = 0.01$.

Table 10. Correlation dependencies between the studied biometric indicators and the SAVI by recording date in the 2022–2023 growing season.

	LS	NSS	NGS	WGS	M1000
SAVI 21.11.22	-	-	-	-	-
SAVI 09.12.22	−0.509	−0.443	0.318	**0.993** **	0.348
SAVI 22.12.22	−0.531	−0.657	**−0.996** **	−0.388	0.735
SAVI 06.01.23	−0.524	−0.626	**−0.993** **	−0.443	0.692
SAVI 20.01.23	−0.270	−0.278	−0.820	−0.736	0.309
SAVI 24.02.23	−0.198	0.039	−0.118	−0.361	−0.162
SAVI 21.03.23	−0.446	−0.236	−0.349	−0.285	0.120
SAVI 25.03.23	−0.522	−0.591	**−0.977** *	−0.488	0.641
SAVI 09.04.23	−0.472	−0.384	−0.727	−0.526	0.347
SAVI 14.04.23	−0.260	−0.281	−0.834	−0.743	0.321
SAVI 23.04.23	0.021	−0.019	−0.698	−0.899	0.084
SAVI 30.04.23	0.509	0.443	−0.318	**−0.993** **	−0.348
SAVI 05.05.23	**0.978** *	0.923	0.699	−0.265	−0.858
SAVI 12.05.23	−0.415	−0.138	0.173	0.252	−0.040
SAVI 19.05.23	−0.415	−0.454	0.238	**0.965** *	0.423
SAVI 01.06.23	−0.756	−0.539	−0.206	0.316	0.384
SAVI 08.06.23	−0.552	−0.295	−0.049	0.174	0.128
SAVI 15.06.23	−0.353	−0.083	0.379	0.463	−0.099
SAVI 22.06.23	0.568	0.708	**0.991** **	0.306	−0.788
SAVI 29.06.23	0.614	0.554	0.823	0.408	−0.525

LS represents the length of the spike, NSS is the number of spikelets per spike, NGS is the number of grains per spike, WGS is the weight of grains per spike, and M1000 is the thousand-kernel weight. Strong dependencies are indicated with an asterisk (*). The correlation levels are as follows: for LS, R is 0.978; NGS, R ranges from 0.977 to 0.996; for WGS, R ranges from 0.965 to 0.993. Significance levels (p-values) are classified as follows: * $p = 0.05$; ** $p = 0.01$.

The potential of using vegetation indices to predict crop productivity has been extensively investigated across different crops and methodologies. For instance, in [37],

the variation of the NDVI in 24 common wheat genotypes under both dry and irrigated conditions was monitored, revealing a positive and reliable correlation between the NDVI and grain yield throughout most of the growing season, except during the spindle and grain-filling stages. Higher correlation coefficients were observed in the drought treatment, while irrigation significantly reduced these coefficients across both experimental sites. Our findings corroborate this study, as precipitation during the growing season caused significant shifts in the NDVI values, depending on the genotype under examination. Similarly, the studies by [38,39] found strong correlations between grain yield and the NDVI across five distinct growing seasons, and [40] highlighted the crucial relationship between biomass and yield formation.

An innovative approach for wheat yield estimation in Latvia was introduced by Vannoppen et al. [41], utilizing NDVI time series to determine the meteorological variables that influence wheat yield. This study employed regional climate models ALARO-0 and REMO (RCM) to achieve this. In another study, [42] applied Pearson's correlation and linear regression analyses to establish relationships between cereal yield and MODIS NDVI data in the Fes-Meknes region of Morocco. While these studies provide promising results for forecasting cereal grain yield, they focus on large-scale regions and are not directly applicable to small experimental plots with varying cereal varieties. Similar to our research, [43] proposed a combined approach for wheat yield prediction by evaluating crop spectral features and agronomic trait parameters. A related study by [44] verified sixteen vegetation indices using correlation analysis and extracted eight textural features from five single spectral bands across three fertility periods. Additionally, [45] presented an approach for estimating crop yield using multispectral (MS) and hyperspectral (HS) imagery from UAVs at different growth stages of winter wheat. Feng et al. [46] also proposed a combined monitoring approach, utilizing various vegetation indices and red-edge parameters based on canopy reflectance from near-surface hyperspectral data and UAV imagery to estimate wheat yield at various growth stages.

In line with our study, [47] quantified yield variations due to temperature and genotype differences within a standard field breeding trial. Although the research was extensive, the findings pertain specifically to a particular wheat genotype in China and may not be directly applicable to breeders and farmers in Europe under differing agrometeorological conditions.

The key innovation of our research lies in the development of a comprehensive methodological framework for distinguishing growth patterns in winter wheat varieties through UAV-based imaging. Our approach examines the correlation between spectral reflectance data and various phenological, biometric, and physiological indicators under specific agroclimatic conditions unique to a particular geographic region. This methodology allows for the scalability of technology using UAVs. Moreover, the proposed framework for interpreting biometric indicators and vegetation reflectance indices is enriched with additional meteorological data collection. All meteorological data were analyzed to derive the relationships between environmental conditions and crops yield.

3.5. Practical Applications of the Proposed Methodology

The proposed methodology for remote monitoring of winter wheat crops using UAVs equipped with multispectral cameras can be valuable for both breeders and farmers when making informed management decisions. Real-time observation of various wheat varieties through the analysis of indices such as the NDVI, SAVI, and EVI2 will assist breeders in the early detection of stress factors, including diseases, weed infestations, and nutrient or water deficiencies. The collected data on the growth and development of wheat varieties under varying meteorological conditions will enable breeders to identify and develop more productive and resilient varieties tailored to specific agricultural regions.

Monitoring the dynamics of vegetation indices throughout the season will aid farmers in the Dobruja region in forecasting the yield of cultivated wheat varieties, optimizing harvest timing, minimizing losses, and maximizing yields.

Furthermore, the spectral indices obtained can provide farmers with precise insights into the extent of poor grain fill under extreme meteorological conditions, such as drought or excessive rainfall, allowing them to make informed decisions regarding additional investments, such as whether to apply fertilization.

This methodology is particularly valuable for small- and medium-sized farmers seeking to incorporate innovative technologies into their agricultural practices, thereby enhancing production efficiency and reducing costs.

This research creates a database regarding the specific trends of change in winter wheat varieties in the agroclimatic conditions of Dobruja and will serve as a benchmark in subsequent experiments.

4. Conclusions

The investigated cultivars follow identical trends in their vegetative development, as established through spectral vegetation indices, with significant differences observed in the early stages (sprouting–spindling) and the late stages of development (post-milk maturity).

Different growing conditions result in varying biometric indicator values, demonstrating that meteorological factors, particularly precipitation, play a fundamental role in determining productivity.

The spectral indices give an accurate picture of the vegetative development of wheat, but the dependencies with the biometric data show that they can only be used as a guide in terms of productivity. This shows that the values of the NDVI, EVI2, and SAVI can be used to predict the productive possibilities, but only after considering the meteorological conditions of the respective growing season.

The primary limiting factor for UAV observations is wind gusts; however, during our study, wind did not significantly affect image capture using a small UAV. In flights conducted with the DJI Mavic 2 Pro, unsuccessful flights due to wind gusts accounted for only 0.059% of the total. In contrast, no unsuccessful flights were recorded with the DJI Phantom 4 Pro, although one flight experienced wind interference, resulting in a deviation from the planned flight path. Despite this, complete data for the observed field were successfully collected. These results demonstrate the reliability of UAV-based remote sensing in varying meteorological conditions, even when wind gusts are present, thereby reinforcing the applicability of this methodology for agricultural monitoring.

The proposed methodology gives accurate results on small areas with a resolution of 0.40 cm/pixel when flying at an altitude of 12 m and 2.3 cm/pixel when flying at an altitude of 100 m. The precision of small and ultra-small agricultural areas makes it suitable for use in wheat selection activities, where the trial is sown at a width of 1.2 m, and the low resolution allows diagnosis of each leaf of the wheat.

Among the NDVI, EVI2, and SAVI considered, the strongest correlation was observed with NGS and WGS. The number of grains and their weight (size) contribute to a larger reflective surface, which in turn enhances the accuracy of the information derived from these indices. This finding underscores the importance of grain characteristics in improving the reliability of vegetation indices for assessing wheat development.

Our future research on the investigated topic will be focused on applying the proposed methodology to other cereal crops. An experiment has been planned for the next three years to validate the data and establish correlation dependencies between vegetation indices and agronomic indicators.

Author Contributions: Conceptualization, A.I.A. and H.P.S.; methodology, A.I.A.; software, A.I.A.; validation, A.I.A., A.Z.A. and H.P.S.; formal analysis, A.I.A. and H.P.S.; investigation, A.I.A.; resources, A.Z.A.; data curation, A.I.A. and H.P.S.; writing—original draft preparation, A.I.A. and H.P.S.; writing—review and editing, A.Z.A.; visualization, A.I.A.; supervision, A.Z.A.; project administration, A.Z.A.; funding acquisition, A.Z.A. All authors have read and agreed to the published version of the manuscript.

Funding: This study was financed by the European Union NextGenerationEU scheme, through the National Recovery and Resilience Plan of the Republic of Bulgaria, project № BG-RRP-2.013-0001-C01.

Data Availability Statement: The data presented in this study are available on request from the corresponding author.

Acknowledgments: The authors are very grateful to the anonymous reviewers whose valuable comments and suggestions improved the quality of the paper.

Conflicts of Interest: The authors declare no conflicts of interest.

References

1. Frazier, B.E.; Walters, C.S.; Perry, E.M.; Pierce, F.J.; Sadler, E.J. Role of remote sensing in site-specific management. In *The State of Site Specific Management for Agriculture*; Pierce, F.J., Sadler, E.J., Eds.; American Society of America: Manhattan, NY, USA, 1997; pp. 149–160. [CrossRef]
2. Panda, S.S.; Hoogenboom, G.; Paz, J.O. Remote Sensing and Geospatial Technological Applications for Site-specific Management of Fruit and Nut Crops: A Review. *Remote Sens.* **2010**, *2*, 1973–1997. [CrossRef]
3. Sishodia, R.P.; Ray, R.L.; Singh, S.K. Applications of Remote Sensing in Precision Agriculture: A Review. *Remote Sens.* **2020**, *12*, 3136. [CrossRef]
4. Asrar, G.; Fuchs, M.; Kanemasu, E.T.; Hatfield, J.L. Estimating absorbed photosynthetic radiation and leaf area index from spectral reflectance in wheat. *Agron. J.* **1984**, *76*, 300–306. [CrossRef]
5. Adão, T.; Hruška, J.; Pádua, L.; Bessa, J.; Peres, E.; Morais, R.; Sousa, J.J. Hyperspectral Imaging: A Review on UAV-Based Sensors, Data Processing and Applications for Agriculture and Forestry. *Remote Sens.* **2017**, *9*, 1110. [CrossRef]
6. Qiao, L.; Tang, W.; Gao, D.; Zhao, R.; An, L.; Li, M.; Sun, H.; Song, D. UAV-based chlorophyll content estimation by evaluating vegetation index responses under different crop coverages. *Comput. Electron. Agric.* **2022**, *196*, 106775. [CrossRef]
7. Li, J.; Veeranampalayam-Sivakumar, A.N.; Bhatta, M.; Garst, N.D.; Stoll, H.; Stephen Baenziger, P.; Belamkar, V.; Howard, R.; Ge, Y.; Shi, Y. Principal variable selection to explain grain yield variation in winter wheat from features extracted from UAV imagery. *Plant Methods* **2019**, *15*, 123. [CrossRef]
8. Lyu, X.; Du, W.; Zhang, H.; Ge, W.; Chen, Z.; Wang, S. Classification of Different Winter Wheat Cultivars on Hyperspectral UAV Imagery. *Appl. Sci.* **2024**, *14*, 250. [CrossRef]
9. Yin, Q.; Zhang, Y.; Li, W.; Wang, J.; Wang, W.; Ahmad, I.; Zhou, G.; Huo, Z. Estimation of Winter Wheat SPAD Values Based on UAV Multispectral Remote Sensing. *Remote Sens.* **2023**, *15*, 3595. [CrossRef]
10. Zu, J.; Yang, H.; Wang, J.; Cai, W.; Yang, Y. Inversion of winter wheat leaf area index from UAV multispectral images: Classical vs. deep learning approaches. *Front. Plant Sci.* **2024**, *15*, 367828. [CrossRef]
11. Li, Z.; Chen, Z.; Cheng, Q.; Duan, F.; Sui, R.; Huang, X.; Xu, H. UAV-Based Hyperspectral and Ensemble Machine Learning for Predicting Yield in Winter Wheat. *Agronomy* **2022**, *12*, 202. [CrossRef]
12. Mohammadi, S.; Uhlen, A.K.; Lillemo, M.; Åshild, E.; Shafiee, S. Enhancing phenotyping efficiency in faba bean breeding: Integrating UAV imaging and machine learning. *Precis. Agric.* **2024**, *25*, 1502–1528. [CrossRef]
13. Wang, I.; Lou, Y.; Wang, W.; Liu, S.; Zhang, H.; Hui, X.; Wang, Y.; Yan, H.; Maes, W. A robust model for diagnosing water stress of winter wheat by combining UAV multispectral and thermal remote sensing. *Agric. Water Manag.* **2024**, *291*, 108616. [CrossRef]
14. Costa, L.; McBreen, J.; Ampatzidis, Y.; Jia Guo, J.; Gahrooei, M.; Babar, M. Using UAV-based hyperspectral imaging and functional regression to assist in predicting grain yield and related traits in wheat under heat-related stress environments for the purpose of stable yielding genotypes. *Precis. Agric.* **2022**, *23*, 622–642. [CrossRef]
15. Baumgardner, M.F.; Sylva, L.F.; Biehl, L.L.; Stoner, E.R. Reflectance Properties of Soil. *Adv. Agron.* **1985**, *38*, 1–44. [CrossRef]
16. Heiden, U.; d'Angelo, P.; Schwind, P.; Karlshöfer, P.; Müller, R.; Zepp, S.; Wiesmeier, M.; Reinartz, P. Soil Reflectance Composites—Improved Thresholding and Performance Evaluation. *Remote Sens.* **2022**, *14*, 4526. [CrossRef]
17. Abdulraheem, M.I.; Zhang, W.; Li, S.; Moshayedi, A.J.; Farooque, A.A.; Hu, J. Advancement of Remote Sensing for Soil Measurements and Applications: A Comprehensive Review. *Sustainability* **2023**, *15*, 15444. [CrossRef]
18. Guan, S.; Fukami, K.; Matsunaka, H.; Okami, M.; Tanaka, R.; Nakano, H.; Sakai, T.; Nakano, K.; Ohdan, H.; Takahashi, K. Assessing Correlation of high-resolution NDVI with fertilizer application level and yield of rice and wheat crops using small UAVs. *Remote Sens.* **2019**, *11*, 112. [CrossRef]
19. Khan, Z.; Chopin, J.; Cai, J.; Eichi, V.-R.; Haefele, S.; Miklavcic, S.J. Quantitative Estimation of Wheat Phenotyping Traits Using Ground and Aerial Imagery. *Remote Sens.* **2018**, *10*, 950. [CrossRef]
20. Miklavcic, S.J.; Chopin, J.; Laga, H. Image-Based Phenotyping Study of Wheat Growth and Grain Yield Dependence on Environmental Conditions and Nitrogen Usage in a Multi-Year Field Trial. *Sustainability* **2024**, *16*, 3728. [CrossRef]
21. Zsebő, S.; Bede, L.; Kukorelli, G.; Kulmány, I.M.; Milics, G.; Stencinger, D.; Teschner, G.; Varga, Z.; Vona, V.; Kovács, A.J. Yield Prediction Using NDVI Values from GreenSeeker and MicaSense Cameras at Different Stages of Winter Wheat Phenology. *Drones* **2024**, *8*, 88. [CrossRef]
22. Rippa, M.; Di Mola, I.; Ottaiano, L.; Cozzolino, E.; Mormile, P.; Mori, M. Infrared Thermography Monitoring of Durum and Common Wheat for Adaptability Assessing and Yield Performance Prediction. *Plants* **2024**, *13*, 836. [CrossRef]

23. Mihaylov, R.; Atanasov, A.; Ivanova, A.; Marinov, A.; Zahariev, S. Tracking the Development of Six Wheat Varieties Using Infrared Imaging and Image Processing Algorithms. In Proceedings of the International Conference of Automatics and Informatics, Varna, Bulgaria, 1–3 October 2020.
24. Atanasov, A.; Mihaylov, R.; Mihova, G. Investigating the possibility of monitoring the drying in the upper soil layer by means of a drone in the Dobruja region. In Proceedings of the 2022 International Conference Automatics and Informatics (ICAI), Varna, Bulgaria, 6–8 October 2022; pp. 115–119. [CrossRef]
25. Mihaylov, R.; Atanasov, A.; Stoyanov, H.; Paskaleva, S. Study of the specifics of the spectral reflections of different varieties of cereals harvest 2021, obtained from the visible and near infrared (NIR) frequency. In Proceedings of the International IEEE Conference "Automatics and Informatics'2021", Varna, Bulgaria, 30 September–2 October 2021.
26. Atanasov, A.; Bankova, A.; Zhecheva, G. Observation of the vegetation processes of agricultural crops using small unmanned aerial vehicles in Dobrudja region. *Bulg. J. Agric. Sci.* **2023**, *29*, 176–181.
27. Atanasov, A.; Bankova, A.; Zhecheva, G. Result Processing Methodology for the Vegetation Processes Remote Sensing by a Small Unmanned Aerial Vehicle. *Bulg. J. Agric. Sci.* **2023**, *29*, 564–569.
28. Survey3: Multispectral Survey Cameras. Available online: https://www.mapir.camera/pages/survey3-cameras (accessed on 10 May 2024).
29. dji.com. 2024. Available online: https://www.dji.com/bg/mavic-2 (accessed on 12 April 2024).
30. pix4d. 2024. Available online: https://www.pix4d.com/product/pix4dcapture (accessed on 23 May 2024).
31. Imagej. 2024. Available online: https://imagej.net/ij/ (accessed on 13 May 2024).
32. Rouse, J.W.; Haas, R.H.; Schell, J.A.; Deering, D.W.; Harlan, J.C. *Monitoring the Vernal Advancement of Retrogradation of Natural Vegetation*; NASA/GSFC: Greenbelt, MD, USA, 1974; p. 371.
33. Huete, A.R. A soil-adjusted vegetation index (SAVI). *Remote Sens. Environ.* **1988**, *25*, 295–309. [CrossRef]
34. Jiang, Z.Y.; Huete, A.R.; Didan, K.; Miura, T. Development of a two-band enhanced vegetation index without a blue band. *Remote Sens. Environ.* **2008**, *112*, 3833–3845. [CrossRef]
35. IBM. 2024. Available online: https://www.ibm.com/products/spss-statistics (accessed on 12 April 2024).
36. Meteoblue. 2024. Available online: https://www.meteoblue.com/bg (accessed on 12 June 2024).
37. Naser, A.Y.; Dahmash, E.Z.; Al-Rousan, R.; Alwafi, H.; Alrawashdeh, H.M.; Ghoul, I.; Abidine, A.; Bokhary, M.A.; Al-Hadithi, H.T.; Ali, D.; et al. Mental health status of the general population, healthcare professionals, and university students during 2019 coronavirus disease outbreak in Jordan: A cross-sectional study. *Brain Behav.* **2020**, *10*, e01730. [CrossRef]
38. Gozdowski, D.; Stępień, M.; Panek, E.; Varghese, J.; Bodecka, E.; Rozbicki, J.; Samborski, S. Comparison of winter wheat NDVI data derived from Landsat 8 and active optical sensor at field scale. *Remote Sens. Appl. Soc. Environ.* **2020**, *20*, 100409. [CrossRef]
39. Panek, E.; Gozdowski, D. Analysis of relationship between cereal yield and NDVI for selected regions of Central Europe based on MODIS satellite data. *Remote Sens. Appl. Soc. Environ.* **2020**, *17*, 100286. [CrossRef]
40. Trentin, G.; Lucato, V.; Sforza, E.; Bertucco, A. Stabilizing autotrophic cyanophycin production in continuous photobioreactors. *Algal Res.* **2021**, *60*, 102518. [CrossRef]
41. Vannoppen, A.; Gobin, A.; Kotova, L.; Top, S.; De Cruz, L.; Vīksna, A.; Aniskevich, S.; Bobylev, L.; Buntemeyer, L.; Caluwaerts, S.; et al. Wheat Yield Estimation from NDVI and Regional Climate Models in Latvia. *Remote Sens.* **2020**, *12*, 2206. [CrossRef]
42. Belmahi, M.; Hanchane, M.; Krakauer, N.Y.; Kessabi, R.; Bouayad, H.; Mahjoub, A.; Zouhri, D. Analysis of Relationship between Grain Yield and NDVI from MODIS in the Fez-Meknes Region, Morocco. *Remote Sens.* **2023**, *15*, 2707. [CrossRef]
43. Zhou, H.; Yang, J.; Lou, W.; Sheng, L.; Li, D.; Hu, H. Improving grain yield prediction through fusion of multi-temporal spectral features and agronomic trait parameters derived from UAV imagery. *Front. Plant Sci.* **2023**, *14*, 1217448. [CrossRef] [PubMed]
44. Kang, Y.; Wang, Y.; Fan, Y.; Wu, H.; Zhang, Y.; Yuan, B.; Li, H.; Wang, S.; Li, Z. Wheat Yield Estimation Based on Unmanned Aerial Vehicle Multispectral Images and Texture Feature Indices. *Agriculture* **2024**, *14*, 167. [CrossRef]
45. Liu, Y.; Sun, L.; Liu, B.; Wu, Y.; Ma, J.; Zhang, W.; Wang, B.; Chen, Z. Estimation of Winter Wheat Yield Using Multiple Temporal Vegetation Indices Derived from UAV-Based Multispectral and Hyperspectral Imagery. *Remote Sens.* **2023**, *15*, 4800. [CrossRef]
46. Feng, H.; Tao, H.; Fan, Y.; Liu, Y.; Li, Z.; Yang, G.; Zhao, C. Comparison of Winter Wheat Yield Estimation Based on Near-Surface Hyperspectral and UAV Hyperspectral Remote Sensing Data. *Remote Sens.* **2022**, *14*, 4158. [CrossRef]
47. Cheng, T.; Li, M.; Quan, L.; Song, Y.; Lou, Z.; Li, H.; Du, X. A Multimodal and Temporal Network-Based Yield Assessment Method for Different Heat-Tolerant Genotypes of Wheat. *Agronomy* **2024**, *14*, 1694. [CrossRef]